CFD MODELLING OF SINGLE-PHASE HYDRODYNAMICS AND HEAT TRANSFER IN SOLID SPONGES

Sebastian MEINICKE[1], Thomas WETZEL[1] and Benjamin DIETRICH[1*]

[1] Department of Thermal Process Engineering, Karlsruhe Institute of Technology (KIT), Karlsruhe 76131, GERMANY
*Corresponding author, E-mail address: dietrich@kit.edu

ABSTRACT

Solid sponges are open-celled, highly porous ceramic or metal foams with a large specific surface area. Due to these properties, such sponges show better ratios of heat transfer and pressure drop, when compared e.g. to conventional packings. If inserted into a reactor or a heat exchanger pipe, the continuity of the solid sponge matrix leads to a much more efficient overall heat supply or withdrawal, respectively. This is why sponges are already used in heat-intensive applications today, such as porous burners and solar receivers. The present paper describes a CFD-based modelling approach for fluid flow and heat transfer in solid sponges. The approach is based on X-ray tomographic (µCT) scans of the original sponge geometry. Adequate choice and reconstruction of so-called representative elementary volumes (REV) of the sponge structure is a crucial first pre-processing step to obtain reliable CFD results at reasonable computational cost. Using open-source software OpenFOAM, a special meshing technique has been developed to get a high-quality computational grid for the selected complex REV geometry sections. CFD modelling is based on the assumption of laminar flow conditions, but specially focusses on handling challenges imposed by the high complexity of the model geometry. A multi-zone approach has been developed to couple hydrodynamics of the scale-resolved REV with an embedding porous zone having equivalent derived resistance properties. It allows specification of enhanced hydrodynamic boundary conditions. Furthermore, the problem of an adequate specification of thermal boundary conditions at the sponge surface has been addressed and discussed. The CFD model presented yields comprehensive results for variable fields inside the sponge structure, which in turn allow derivation of the integral quantities pressure drop (Δp) and interfacial heat transfer coefficient (α_{F-S}). These results agree well with available validation data from literature.

NOMENCLATURE

a edge length [m]
$c_{p,F}$ isobaric specific heat capacity [J kg^{-1} K^{-1}]
d_h hydraulic diameter [m]
F Forchheimer inertial coefficient [-]
Hg Hagen number $\left(=(\Delta p/\Delta L)\cdot\left(d_h^{\ 3}/\left(\rho_F\cdot v_F^{\ 2}\right)\right)\right)$ [-]
k heat transition coefficient [W m^{-2} K^{-1}]
K permeability [m^2]
L length [m]
Nu Nusselt number, $\left(=(\alpha_{F-S}\cdot d_h)/\lambda_F\right)$ [-]

Δp pressure drop [Pa]
p pressure [Pa]
Pr Prandtl number [-]
Re Reynolds number, $\left(=(U_0\cdot d_h)/v_F\right)$ [-]
S_V specific (volumetric) surface area [m^2 m^{-3}]
T temperature [K]
u   velocity [m s^{-1}]
U_0 superficial velocity (magnitude) [m s^{-1}]
V volume [m^3]

α_{F-S} interfacial heat transfer coefficient [W m^{-2} K^{-1}]
β thermal expansion coefficient [K^{-1}]
ψ porosity [-]
ρ density [kg m^{-3}]
λ heat conductivity [W m^{-1} K^{-1}]
v kinematic viscosity [m^2 s^{-1}]

F fluid
S solid
ref   with regard to reference conditions (T_{ref} = 298,15 K)
2Ph with regard to fluid-solid two-phase system

INTRODUCTION

Solid sponges, also referred to as open-celled foams, are considered to be promising materials for use in heat intensive application areas, such as porous burners and volumetric solar receivers (Gauthier et al., 2008; Ávila-Marín, 2011; Becker et al., 2006). Due to their intrinsic high porosity and large specific surface area, such sponges combine low pressure drops with comparably high heat and mass transfer rates (Dietrich et al., 2009; Inayat et al., 2011). Particularly when compared to a conventional loose packing, heat transfer in sponges is primarily enhanced due to the continuity of the solid sponge matrix itself. Using sponge materials with a high solid heat conductivity λ_S helps to fully exploit the superiority of the continuous heat conduction over inter-particle (point-contact) heat transfer in packings. Many authors have addressed hydrodynamic and thermal characterization of well heat-conducting ceramic and metal sponges experimentally. A common approach to present results is to derive integral momentum and heat transfer characteristics of the sponge. The sponges' pressure drop behavior is usually quantified by introducing overall permeability and inertial resistance coefficients, whereas heat transfer description may be generally addressed with two different modelling approaches. The first of them is based on the assumption of a local thermal equilibrium (LTE) at the fluid-solid interface and assumes averaged material properties and variable fields shared by the fluid and the solid sponge phase. In this case, quantitative

thermal characterization of the sponge is performed by introducing the effective heat conductivity λ_{2Ph} (Boomsma and Poulikakos, 2001; Fischedick et al., 2015). In contrast, heterogeneous modelling approaches account for actual local thermal non-equilibrium (LNTE) conditions at the sponge surface by solving two different temperature fields in the fluid and the solid phase and coupling them by means of the interfacial heat transfer coefficient $\alpha_{F\text{-}S}$. Experimental determination of averaged $\alpha_{F\text{-}S}$ values is possible either by using a transient single-blow method (Younis and Viskanta, 1993; Dietrich, 2013), or by applying a steady-state measurement technique, yielding $\alpha_{F\text{-}S}$ as a function of heat conductivity properties of the solid sponge material and at a given wall temperature (Fuller et al., 2005). However, information on temperature field distribution and local heat transfer coefficients may only be accessed by means of numerical simulation (Wu et al., 2011). This has already motivated numerous CFD investigations on single-phase hydrodynamics and heat transfer in solid sponges. Wu and Zhao (2011) investigated pressure drop and convective heat transfer between air flow and ceramic sponges using periodic tetrakaidecahedron cell elements representing the sponge geometry. Using the same idealized modeling geometry, Kopanidis (2010) even modelled conjugate heat transfer between the fluid and solid phase. Other authors (e.g. Petrasch et al., 2008; Bianchi et al., 2015) based their CFD models on X-ray tomographic scans of the real sponge structure and derived pressure drop and interfacial heat transfer coefficient results. All of these publications deal with the problem of specifying adequate boundary conditions, whilst ensuring comparability of the numerical set-up and the according validation experiment.

Since sponge structures are of special interest for high-temperature applications, often combined with high heat transfer rates, this investigation specially focusses on comparably well heat-conducting ceramic SiSiC (= silicon infiltrated silicon carbide) sponges. Following an approach that relies on µCT scans of the real structure of one selected SiSiC sponge type, a suitable CFD model to describe single-phase hydrodynamics and heat transfer inside the porous structure is provided. It is the aim of this study to work out the challenges posed by the complex sponge geometry. Among these are finding an adequate meshing strategy, specifying suitable boundary conditions and deriving meaningful integral parameters, that allow reliable comparison of CFD simulation results to existing experimental and literature data. Beyond, this model also forms the basis for planned future CFD investigations on two-phase flow phenomena in such structures, using a so-called phase-field method approach.

MODEL DESCRIPTION

The central aim of this work is to adequately reproduce hydrodynamics and heat transfer in solid sponges using a scale-resolving CFD modelling approach. This poses the following challenges, which amount to ensuring sufficient modelling accuracy at a reasonable computational cost:

1.) determining an adequately sized and shaped section of the sponge to be numerically investigated

2.) ensuring sufficient mesh resolution, especially nearby the solid sponge surface

3.) specifying suitable and reliable hydrodynamic and thermal boundary conditions

Geometry generation and structural analysis

Simulation geometries were derived from existing µCT scans of small SiSiC sponge samples (size: 20 mm x 40 mm x 40 mm) and included different sponge types with cell densities varying between 10, 20, 30 and 45 ppi (pores per linear inch). An in-house image processing tool using commercial MATLAB software has been developed. It employs several smoothing steps using median and non-linear anisotropic diffusion filters, as well as segmentation methods thresholding and active contours modelling ('snake'). This tool allows the reconstruction of any sponge geometry sections with freely selectable shape (cylindrical, cubic) and size, hereafter referenced to in terms of an equivalent edge length a. In order for the chosen geometry section to be representative of the whole sponge structure, some minimum edge length is required. This quantity may be determined through an additional structural analysis, which the reconstruction tool described allows to be carried out at the same time. It provides characteristic data like the sponge's (volumetric) specific surface area S_V and its porosity ψ. These aforementioned quantities are defined as follows:

$$S_V = \frac{S}{V} = \frac{S}{V_F + V_S} \tag{1}$$

$$\psi = \frac{V_F}{V} = \frac{V_F}{V_F + V_S} \tag{2}$$

Here, V_F and V_S are the partial volumes of the fluid and the solid phase of the sponge section (for its part having a total volume V and surface area S), respectively.

Below, ψ and S_V are used to assess whether the chosen geometry section may be considered to be a representative elementary volume (so-called REV) of the whole sponge. Fig. 1 illustrates the decrease of the variation in ψ and S_V if the geometry section size is increased. Based on this knowledge, a minimum REV edge length a_{REV} may be set.
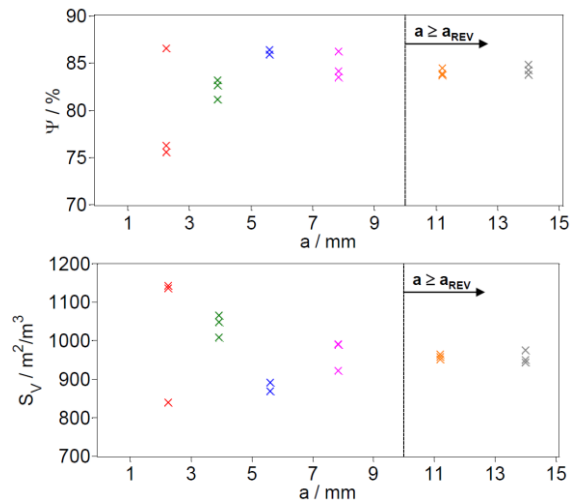
Figure 1: Course of the characteristic quantities S_V and ψ for varying equivalent edge length a of different geometry sections of a 20 ppi SiSiC sponge.

The choice of a_{REV} strongly depends on the sponge type to be investigated and increases with decreasing cell density, the reason for this trend being a decrease in the number of characteristic sponge cell units per volume. Results in Fig.

2

1 refer to the common 20 ppi sponge type. In this case, by restricting the margin of relative fluctuation of ψ and S_V values from structural analysis of different sponge sections to less than 5 %, this minimum edge length is found to be $a_{REV} \approx 10$ mm. In the following, for ease of CFD model set-up and results presentation, considerations are restricted to this exemplary sponge type only. However, findings thus obtained may easily be transferred to other sponge types as well. Furthermore, cylindrically shaped REVs were found to be the most suitable choice for better subsequent classification of simulation results. This is because corresponding validation data was mostly gained from experimental set-ups using cylindrical sponge samples as well.

Since ψ and S_V are both unambiguously determinable by evaluating the stl (= surface tessellation lithography) representation of the sponge REV generated in the preceding image reconstruction step, it is advisable to also use these quantities for the derivation of a reliable and well-reproducible characteristic length of the sponge. It is introduced here as the so-called hydraulic diameter d_h and calculated according to eq. (3) (Dietrich et al., 2009).

$$d_h = \frac{4 \cdot \psi}{S_V} \tag{3}$$

Thus, d_h is also considered to be a suitable choice for the characteristic length used later on for the definitions of dimensionless Reynolds (Re), Hagen (Hg) and Nusselt (Nu) numbers.

Model geometry and boundary condition specification

For reasons of better results transferability and handling geometric irregularity of the REV's boundary patches, the model geometry shown in Fig. 2 is proposed. It consists of a resolved zone representing the sponge REV under investigation and an 'enveloping zone', which allows embedding the REV both in axial and radial direction.
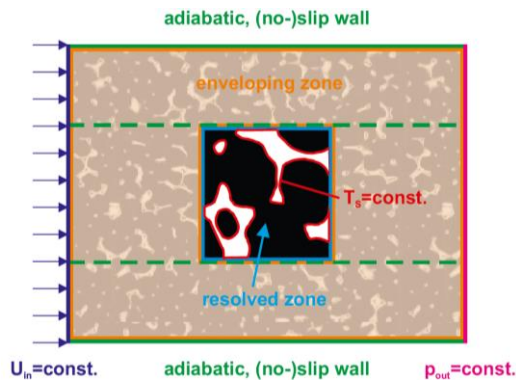

Figure 2: Schematic depiction of modelling geometry. (dashed green line represents only axial embedding case)

First-mentioned 'axial embedding' concept has been assumed by default for all calculations presented in this paper. It enables the specification of radially constant variable distributions at the inlet (fluid inlet velocity $\mathbf{u_{F,in}}$ and inlet temperature $T_{F,in}$) and outlet patch (reference pressure $p_{F,out} \equiv 0$) and helps to preserve flow structures in the upstream and downstream of the resolved REV. However, 'radial embedding' aims at upscaling the REV's relatively small dimensions to much larger dimensions of real reactors or pipes where sponges shall be inserted in practical applications. Thus, a 'real' no-slip wall boundary

condition may be specified at the model geometry's side walls. If embedding is restricted to axial direction only, however, these side walls are treated as inner cut surfaces of the sponge sample and so are assigned a frictionless slip wall boundary condition instead.

The 'enveloping zone' has been modelled both as a flow resistance-free zone or a so-called 'porous zone'. The latter approach is particularly required if the REV is also embedded radially and implies assigning an extra pressure drop $\nabla p_{F,por}$ to the enveloping zone, providing it with similar hydrodynamic properties as the partial calculation for the scale-resolved sponge REV yields (see next subsection, eq. (8)). Thus, flow is prevented from circumventing the 'obstacle' sponge. The general applicability of this method has been proven e.g. by Missirlis et al. (2010), who have developed a similar modelling approach to describe heat transfer and pressure drop in heat exchangers for aero engine applications.

Another important modelling issue is to define an adequate coupling of fluid and solid heat transfer. Fig. 3 schematically shows the heat flow path from (in this case heating) fluid up to surrounding (cooling) reactor wall or pipe wall, respectively. It thereby passes through single heat transfer resistances at the sponge surface (①), in the solid matrix itself (②) and at contact points to the surrounding (③).
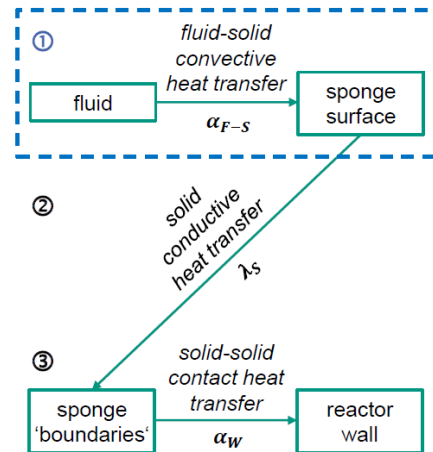
Figure 3: Thermal coupling of fluid and solid sponge

In the first step of thermal CFD modelling within the framework of this project, only the first, blue-coloured link of this transport chain has been considered. This simplification implies the assumption that the second and third links' heat transfer resistances may be neglected as compared to the fluid-solid convective heat transfer resistance being reciprocally proportional to the interfacial heat transfer coefficient α_{F-S}, which is used for its quantification. This assumption may be accounted for in the CFD model set-up by specifying a constant temperature T_S at the sponge's surface (Dirichlet type boundary condition). In this case, by balancing the sponge REV – thereby assuming its side walls to be adiabatic – the calculation term according to eq. (4) may be derived for the product $\alpha_{F-S} \cdot S_V$. It denotes the volumetric interfacial heat transfer coefficient and is proposed for subsequent results presentation, because it is independent of the sponge's geometrical properties.

3

$$\alpha_{F,S} \cdot S_V = \frac{\rho_F \cdot c_{p,F} \cdot U_0 \cdot \ln\left(\frac{\overline{T_{F,in}} - T_S}{\overline{T_{F,out}} - T_S}\right)}{L_{REV}} \quad (4)$$

where U_0 is the superficial fluid velocity magnitude, L_{REV} is the length of the sponge REV in flow direction and $c_{p,F}$ is the isobaric specific heat capacity.

Mesh generation

Another model requirement is to enable high-quality mesh generation for these highly irregularly shaped simulation geometries. Mesh quality may be estimated in terms of reproducibility of ψ and S_V, by comparing values obtained from preceding structural or stl geometry analysis to results from an overall evaluation of all generated computational grid cells yielding 'reference' values for ψ and S_v. Thus, the degree of geometry representation accuracy is given for different mesh settings. Table 1 exemplarily points out this aspect for a cylindrical 20 ppi SiSiC sponge REV ($a_{REV,eq} \approx 0.01$ m, from structural analysis: $S_{V,geom} = 1064$ m^2 m^{-3}, $\psi_{geom} = 84.44$ %). As can be seen from Table 1, increasing overall mesh resolution, especially nearby the sponge surface, allows to capture more details of the underlying stl geometry ($S_V \rightarrow S_{V,geom}$). However, even the most elaborate meshes' ψ and S_V values are still lower than the corresponding values obtained from stl geometry analysis. This underestimation may be attributed to the original sponge geometry's disjointed inner porosities, which cannot be resolved by this approach relying on a continuous mesh representation. In fact, since these inner porosities are not directly (hydrodynamically) accessible by the fluid, this difference has no effect on CFD calculations carried out in this work.

Table 1: Influence of selected meshing parameters (core cells' size (*ccs*), refinement level at sponge surface (*ssrf*), corresponding to a local cell size $lcs = (ccs) \cdot 2^{(-ssrf)}$ at the sponge surface) on effective ψ and S_V of the mesh.

ccs [mm]	0.4		0.2		0.1		0.05	
	ψ [%]	S_V [m^{-1}]	ψ [%]	S_V [m^{-1}]	ψ [%]	S_V [m^{-1}]	ψ [%]	S_V [m^{-1}]
ssrf [-]								
1	82.90	933.4	82.69	947.3	82.66	964.5	82.65	964.3
2	82.70	946.7	82.65	964.5	82.65	986.2	(∗)	(∗)
3	82.66	963.6	82.65	986.5	82.65	1006	(∗)	(∗)
4	82.65	985.8	82.65	1006	(∗)	(∗)	(∗)	(∗)
5	82.63	1005	(∗)	(∗)	(∗)	(∗)	(∗)	(∗)

(∗): unreasonably high computational costs (> 50 millions of cells)

Apart from that, subsequent mesh-independency study of results for pressure drop (Δp) and interfacial heat transfer coefficient (α_{F-S}) with these variable mesh settings also confirmed that the degree of geometric originality should be as high as possible to obtain reliable simulation results.

Governing equations

Single-phase CFD modelling is based on the assumption of steady-state, laminar and incompressible flow conditions. Thermal modelling of the fluid comprises the application of the Boussinesq approximation, according to which buoyancy effects are accounted for by a force density source term within the incompressible formulation of the momentum equations. In addition, Newtonian fluid behavior is assumed. This leads to the simplified set of conservation equations given by eq. (5) - (7).

$$\nabla \cdot \mathbf{u} = 0 \quad (5)$$

$$\nabla \cdot (\mathbf{uu}) = -\frac{1}{\rho_{ref}} \nabla p + \nu \Delta \mathbf{u} + \left(1 - \beta(T - T_{ref})\right) g \quad (6)$$

$$\nabla \cdot (\mathbf{u}T) = \frac{\nu}{Pr} \Delta T \quad (7)$$

where p is the pressure, $\mathbf{u}$ is the velocity vector and T is the temperature, using temperature independent fluid properties ν (kinematic viscosity), ρ_{ref} (reference density at reference temperature T_{ref}), β (thermal expansion coefficient) and Pr (Prandtl number). In order for these assumptions to be reasonable, thermal boundary conditions were specified such that only small temperature differences occurred within the fluid domain (corresponding to $T_{F,in} = 298.15$ K and $T_S = 303.15$ K).

The flow inside the porous sponge system is characterized by the Reynolds number $Re = (U \cdot d_h)/\nu_F$, using the hydraulic diameter definition according to eq. (3) and the mean velocity magnitude $U = U_0/\psi$ inside the sponge. A common approach to classify flow regimes inside porous media was presented by Dybbs and Edwards (1984). According to this approach, laminar steady-state flow conditions are assumed if $Re \leq 150$ (Darcian-Forchheimer flow regime). Flow state is still considered to be laminar, but transient if $150 < Re \leq 300$ and only becomes turbulent if $Re > 300$. However, strictly speaking, this classification was only introduced for sphere packings, using the spheres' diameter as a characteristic length for Reynolds number definition. Exact transferability of these proposed Reynolds number ranges to solid sponges is therefore questionable. In this study, the Reynolds number range $25 < Re < 500$ has been investigated. Nevertheless, turbulence modelling is not included in the CFD model presented. This is mainly due to high additional modelling efforts and uncertainties introduced. Not least because of the good convergence behavior observed with the corresponding laminar modelling approach, the authors consider this to be a reasonable assumption, yet being well aware of its simplifying character.

In case the 'porous zone approach' – as described in the previous sub-section – is applied, eq. (6) needs to be modified by adding an extra pressure drop term ∇p_{por}, which may be described in terms of a common Darcy-Forchheimer approach, according to eq. (8):

$$\nabla p_{por} = -\left(\frac{\nu\rho}{K}\mathbf{u} + \frac{F\rho}{\sqrt{K}}|\mathbf{u}|\mathbf{u}\right) \quad (8)$$

where K is Darcy's permeability and F is the Forchheimer inertial coefficient. Initial values for coefficients K and F have been derived from an existing literature correlation (Dietrich et al., 2009) and then adapted iteratively to pressure drop behavior of the scale-resolved sponge REV. Therefore, pressure drop results from the preceding calculation loop have been plotted against investigated superficial velocities U_0, yielding K and F as least square fitting parameters of a second-order polynomial.

Solution procedure

To carry out CFD simulations, the open-source software OpenFOAM® (v2.3.0) was used. Due to the required high spatial resolution nearby the sponge surface and minimum REV size, calculations had to be performed on grids consisting of up to 30 million cells to yield reliable results.

The semi-implicit method for pressure-linked equations (SIMPLE) was used to realize pressure-velocity coupling for steady-state CFD calculations. Using a 20-core CPU with 128 GB RAM, parallelized steady-state calculations took approximately 4 h each. The solution was considered to be well converged when reaching residual values of 10^{-5} for each flow variable.

RESULTS

Results for single-phase pressure drop (Δp) were obtained by axially embedding a cylindrical sponge REV (with radius $r_{REV} = 6$ mm and length $L_{REV} = 10$ mm). Depending on whether the 'porous zone' approach described above was applied or not, OpenFOAM solvers *simpleFoam* or *porousSimpleFoam* were used to solve equations (5) and (6) in case of isothermal flow conditions ($T \equiv T_{ref} =$ const.). However, heat transfer calculations at non-isothermal conditions required use of the *buoyantBoussinesqSimpleFoam* solver in order to additionally solve eq. (7).
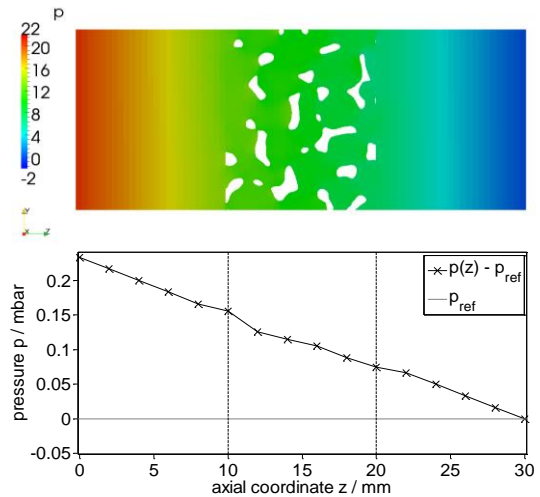
Pressure drop

Static pressure contour plots in Fig. 4 and Fig. 5 are both recorded in the YZ center plane of the cylindrical modelling geometry, parallel to the main flow direction. Fig. 4 presents static pressure distribution results in case the REV is embedded into a flow resistance-free surrounding.
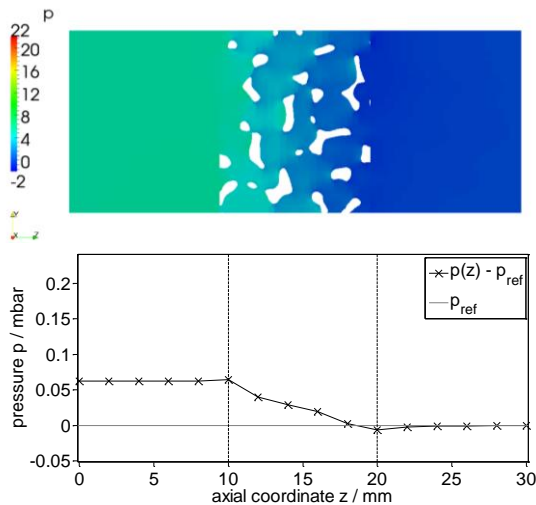

Figure 4: YZ cutting plane contour plot (top) and axial distribution of cross-section average (below) of static pressure, using *simpleFoam* solver ($U_0 = 0.8$ m s^{-1})

The axial distribution of cross-section averaged pressure (plotted in Fig. 4, below) illustrates that pressure gradient across the REV is nearly constant and only slightly fluctuating. The same trend was observed e.g. by Wu et al. (2011). However, a slightly negative pressure has been observed in the REV's outlet interface, which may have undesirable effects on the CFD calculation like e.g. artificial backflow into the REV. Fig. 5 shows that this unphysical flow behavior is avoided if the 'porous zone' modelling approach is applied. Furthermore, Fig. 5 indicates the extra 'porous' pressure drop of the enveloping zone according to eq. (8). It can be seen that iterative fitting of parameters A and B to available pressure drop results of the REV allows extrapolation of the same pressure gradient also to the porous surrounding.

Figure 5: YZ cutting plane contour plot (top) and axial distribution of cross-section average (below) of static pressure, using *porousSimpleFoam* solver ($U_0 = 0.8$ m s^{-1})

Fig. 6 shows pressure drop results obtained from these two hydrodynamic modelling approaches in dimensionless form (Re vs. Hg number plot). For comparison, results from own measurements as well as from a literature correlation, being applicable to all ceramic sponge types (Dietrich et al., 2009), are displayed as well.
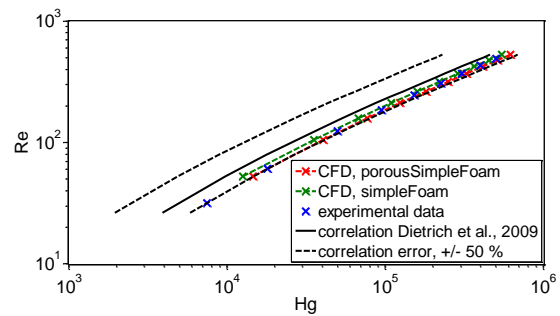
Figure 6: Dimensionless pressure drop simulation results from resistance-free and porous resistance surrounding zones modelling approaches, compared with experimental and literature data (for SiSiC, 20 ppi sponge)

CFD simulation results were found to agree well with data from experimental pressure drop measurements on exactly the same sponge samples, which have also been used for geometry generation and CFD model deduction. Indeed, considering results in the context of existing literature suggests that the CFD model tends to slightly overestimate the pressure drop, especially if the 'porous zone approach' is applied. This might be due to implied flow deceleration at the REV's transition area to the downstream embedding zone. Ongoing work therefore focusses on extending this model in such a manner as to allow local adaption of the porous zone's flow resistance to the computed velocity field in the vicinity of its shared interfaces with the scale-resolved REV. Thus, smooth transition of flow fields may be assured. However, it has to be kept in mind that the literature correlation's uncertainty is quite high (≈ 40 %) due to its overall validity for all sponge types, which is in contrast to consistency of experimental and numerical investigations presented. Table 2 quantifies and compares results by specifying values and relative deviations of the Darcian and Forchheimer coefficients K and F.

Table 2: Coefficients K and F, calculated from literature correlation and second-order polynomial fitting of simulation results and experimental data, and their relative deviations with respect to values from experimental data.

	K [m^2]	F [-]	ΔK [%]	ΔF [%]
CFD results, *porousSimpleFoam*	$5.33 \cdot 10^{-8}$	$1.70 \cdot 10^{-1}$	11.04	18.88
CFD results, *simpleFoam*	$6.06 \cdot 10^{-3}$	$1.60 \cdot 10^{-1}$	26.25	11.89
experimental data	$4.80 \cdot 10^{-8}$	$1.43 \cdot 10^{-1}$	-	-
literature correlation (Dietrich et al., 2009)	$9.57 \cdot 10^{-8}$	$1.77 \cdot 10^{-1}$	99.38	23.78

Heat transfer

The thermal CFD modelling approach as described above yields the fluid temperature field inside the sponge as a direct result of the simulation. By averaging over the REV's outlet patch, the flow-averaged outlet temperature $\overline{T_{F,out}}$ is obtained. $\overline{T_{F,out}}$ is in turn needed to calculate the interfacial heat transfer coefficient α_{F-S} according to eq. (4). For a more general evaluation, the results in Fig. 7 are again presented in dimensionless form (*Nu* vs. *Re* plot).
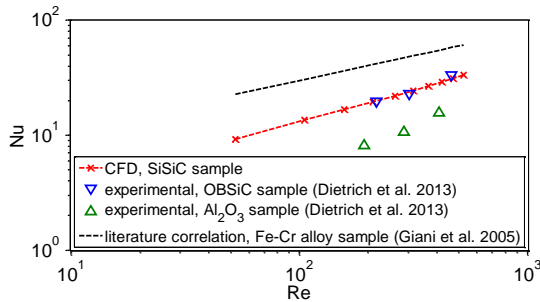
Figure 7: Dimensionless representation of CFD results for interfacial heat transfer coefficient (SiSiC, 20 ppi sponge), compared with literature data (similar sponge types).

In the absence of directly comparable validation data, calculated interfacial heat transfer coefficient values for varying inlet velocities have been compared to trends reported in similar experimental studies, showing a good agreement with them (Dietrich, 2013; Giani et al., 2005). Although results are in the same order of magnitude, Fig. 7 also indicates discrepancies in their absolute amount. These minor deficiencies may probably be ascribed to the current simplifying assumption of a constant sponge surface temperature T_S. This assumption implies an infinite heat conductivity of the solid SiSiC sponge matrix. In contrast, experimental measurements by Dietrich (2013) were performed with relatively low conductive OBSiC (= oxidic bonded SiC) sponges and Al$_2$O$_3$ sponges. Although investigated SiSiC sponges and particularly Fe-Cr alloy sponges investigated by Giani et al. (2005) display considerably higher heat conductivities, results are still not directly comparable. Table 3 states geometrical properties and heat conductivity of all relevant sponge types. While values ψ and S_V derived from preceding structural analysis clearly indicate geometrical similarity of investigated SiSiC, OBSiC and Al$_2$O$_3$ sponges, no metal sponge displaying better geometrical accordance could be found in literature.

Table 3: Geometrical properties *ppi*, ψ, S_V and solid heat conductivities λ of sponges investigated.

	ppi [-]	ψ [%]	S_V [m^2 m^{-3}]	λ [W m^{-1} K^{-1}]
CFD, SiSiC	20	84.75	962.04	$\to \infty$ (∗)
exp., OBSiC	20	84.5	890	18.88
exp., Al$_2$O$_3$	20	85.4	974	9.2
corr., Fe-Cr alloy	12.8	93.7	767	27.5

(∗): implied by assumption of constant sponge surface temperature

Due to this evident lack of direct comparability with existing experimental data, current model development also includes meshing the solid sponge matrix and solving the heat conduction equation for it. Thermal boundary condition specification for the sponge may thus be shifted to its outer boundaries, which allows a slightly modified definition of the overall heat transition coefficient k. Based on eq. (4) k could then be calculated by simply substituting T_S with the wall temperature T_W. At the same time, CFD model set-up needs to be modified such that – by defining multiple fluid and solid regions and coupling them with suitable thermal transition conditions – conjugated heat transfer calculations may be carried out (Kopanidis et al., 2010). Although these model extensions have already been preliminarily implemented, reliable results for k are not yet available.

CONCLUSION

Single-phase hydrodynamics and heat transfer in solid sponges have been numerically investigated using a scale-resolving CFD modelling approach. Starting with a detailed structural analysis of available µCT data, so-called REVs (= representative elementary volumes) of the sponge structure of interest have been reconstructed in a geometry format usable for CFD simulation. Actual CFD model set-up has been implemented in OpenFOAM® and focussed on well heat conducting SiSiC, 20 ppi sponge type. Embedding the sponge REV into a larger enveloping zone and assigning according flow resistance properties to it, allows a reliable specification of needed hydrodynamic and thermal boundary conditions. However, thermal CFD model set-up was restricted to solid-fluid interfacial heat transfer only, yielding pressure drop Δp and heat transfer coefficient α_{F-S} as significant results of the simulation. Results have then been compared to own experimental measurements using exactly the same sponge samples and to available data from the literature. Concerning pressure drop results, a very good agreement with the validation data has been found, indicating high hydrodynamic model quality and reliability. Results for interfacial heat transfer coefficient are also consistent with the trends reported in the according literature. However, common experimental set-ups and current status of CFD modelling still lack accurate comparability. This remaining deficiency motivates further enhancements of the presented thermal CFD modelling approach. Instead of restricting modelling considerations to interfacial heat transfer only – which gives rise to the necessity to specify adequate boundary conditions at the sponge surface – a coupled heat transfer modelling for both the fluid and the solid sponge matrix is proposed. This extension allows a reliable definition of the heat transition coefficient k based on the reactor wall temperature T_W, which may easily be reproduced both experimentally and numerically.

REFERENCES

ÁVILA-MARÍN, A.L., (2011), "Volumetric receivers in Solar Thermal Power Plants with Central Receiver System technology: A review", *Sol. Energy,* **5**, 891–910.

BECKER, M. et al., (2006), "Theoretical and numerical investigation of flow stability in porous materials applied as volumetric solar receivers", *Sol. Energy,* **10**, 1241–1248.

BIANCHI, E. et al., (2015), "Numerical simulation of heat transfer in the near-wall region of tubular reactors packed with metal open-cell foams", *Chem. Eng. J.*, 268–279.

BOOMSMA, K. and POULIKAKOS, D., (2001), "On the effective thermal conductivity of a three-dimensionally structured fluid-saturated metal foam", *Int. J. Heat Mass Transfer,* **4**, 827–836.

DIETRICH, B. et al., (2009), "Pressure drop measurements of ceramic sponges—Determining the hydraulic diameter", *Chem. Eng. Sci.,* **16**, 3633–3640.

DIETRICH, B., (2013), "Heat transfer coefficients for solid ceramic sponges – Experimental results and correlation", *Int. J. Heat Mass Transfer*, 627–637.

DYBBS, A. and EDWARDS, R.V., (1984), "A New Look at Porous Media Fluid Mechanics — Darcy to Turbulent", *Fundamentals of Transport Phenomena in Porous Media NATO ASI Series,* **82**, 199-256.

FISCHEDICK, T. et al., (2015), "High temperature two-phase thermal conductivity of ceramic sponges with stagnant fluid – Experimental results and correlation including thermal radiation", *Int. J. Therm. Sci*, 1–11.

FULLER, A.J. et al., (2005), "Measurement and interpretation of the heat transfer coefficients of metal foams", *Mechanical Engineering Science,* **219**, 183–192.

GAUTHIER, S. et al., (2008), "Investigation of the flame structure and nitrogen oxides formation in lean porous premixed combustion of natural gas/hydrogen blends", *Int. J. Hydrogen Energ.,* **18**, 4893–4905.

GIANI, L. et al., (2005), "Heat Transfer Characterization of Metallic Foams", *Ind. Eng. Chem. Res.,* **24**, 9078–9085.

INAYAT, A. et al., (2011), "Determining the specific surface area of ceramic foams: The tetrakaidecahedra model revisited", *Chem. Eng. Sci.,* **6**, 1179–1188.

KOPANIDIS, A. et al., (2010), "3D numerical simulation of flow and conjugate heat transfer through a pore scale model of high porosity open cell metal foam", *Int. J. Heat Mass Transfer,* **11-12**, 2539–2550.

MISSIRLIS, D. et al., (2010), "Numerical development of a heat transfer and pressure drop porosity model for a heat exchanger for aero engine applications", *Applied Thermal Engineering,* **11-12**, 1341–1350.

PETRASCH, J. et al., (2008), "Tomography based determination of permeability, Dupuit–Forchheimer coefficient, and interfacial heat transfer coefficient in reticulate porous ceramics", *Int. J. Heat Fluid Fl.,* **1**, 315–326.

WU, Z. et al., (2011), "Numerical simulation of convective heat transfer between air flow and ceramic foams to optimise volumetric solar air receiver performances", *Int. J. Heat Mass Transfer,* **7-8**, 1527–1537.

WU, Z.G. and ZHAO, C.Y., (2011), "Experimental investigations of porous materials in high temperature thermal energy storage systems", *Sol. Energy,* **7**, 1371–1380.

YOUNIS, L.B. and VISKANTA, R., (1993), "Experimental determination of the volumetric heat transfer coefficient between stream of air and ceramic foam", *Int. J. Heat Mass Transfer,* **6**, 1425–1434.